PERGAMON

Chemical Engineering Science 56 (2001) 813–821

Chemical Engineering Science

www.elsevier.nl/locate/ces

Radial and axial dispersion of the liquid phase within a KATAPAK-S® structure: experiments vs. CFD simulations

J. M. van Baten, J. Ellenberger, R. Krishna*

Department of Chemical Engineering, University of Amsterdam, Nieuwe Achtergracht 166, 1018 WV Amsterdam, Netherlands

Abstract

The radial, and axial, liquid-phase dispersion within the catalytically packed criss-crossing sandwich structures of KATAPAK-S has been studied experimentally with the use of computational fluid dynamics (CFD). The KATAPAK-S structure has excellent radial dispersion characteristics. The radial dispersion coefficient in such structures is about one order of magnitude higher than that for conventional packed (trickle) beds. The CFD simulations of the radial dispersion are in good agreement with experiments. At high-liquid loads, there is liquid flow outside the wire gauze envelopes, leading to enhanced axial dispersion. The axial dispersion coefficient of the liquid phase of KATAPAK-S is of the same order of magnitude as the radial dispersion coefficient.

Keywords: Structured packing; Residence time distribution; Computational fluid dynamics; Radial dispersion; Axial dispersion

1. Introduction

For heterogeneously catalysed reactive distillation processes, hardware design poses considerable challenges (Taylor & Krishna, 2000). The catalyst particle sizes used in such operations are usually in the 1–3 mm range. Larger particle sizes lead to intra-particle diffusion limitations. To overcome the limitations of flooding during counter-current vapour-liquid contacting, the catalyst particles have to be enveloped within wire gauze structures. Two commonly used structures in industry are described below.

1. Catalyst particles enclosed in cloth wrapped in the form of bales (Johnson & Dallas, 1994; Smith, 1985; Subawalla, Gonzalez, Seibert, & Fair, 1997), see Fig. 1(a).
2. Catalyst particles sandwiched between corrugated sheets of wire gauze (Bart & Landschützer, 1996; Ellenberger & Krishna, 1999; Gelbein & Buchholz, 1991; Van Gulijk, 1998; Higler, Krishna, Ellenberger, & Taylor, 1999; Johnson & Dallas, 1994; Moritz & Hasse, 1999; Stringaro, 1991, 1995), see Fig. 1(b). Such structures are being licensed by Sulzer, called KATAPAK-S, and Koch–Glitsch, called KATAMAX (DeGarmo, Parulekar, & Pinjala, 1992). They consist of two pieces of rectangular crimped wire gauze sealed around the edge, thereby forming a pocket of the order of 1–5 cm wide between the two screens. These catalyst "sandwiches" or "wafers" are then bound together.

An important claimed advantage of the structured criss-crossing catalyst sandwich structures shown in Fig. 1(b) over alternative configurations is with respect to radial distribution of liquid through the packed catalyst channels. The primary objective of our work is to determine the radial liquid residence time distribution in a KATAPAK-S-like structure and compare this with a conventional packed bed without the criss-crossing construction. Besides experimental work, we have also used computational fluid dynamics (CFD) in order to obtain an insight into the liquid flow.

2. Experimental

In Fig. 2, a schematic view of the experimental set-up is shown. Two types of structures were studied: (a) a KATAPAK-S structure and (b) a conventional packed bed.

* Corresponding author. Tel.: +31-20-525-7007; fax: +31-20-525-5604.

E-mail address: krishna@its.chem.uva.nl (R. Krishna).

0009-2509/01/$ - see front matter
PII: S0009-2509(00)00293-1

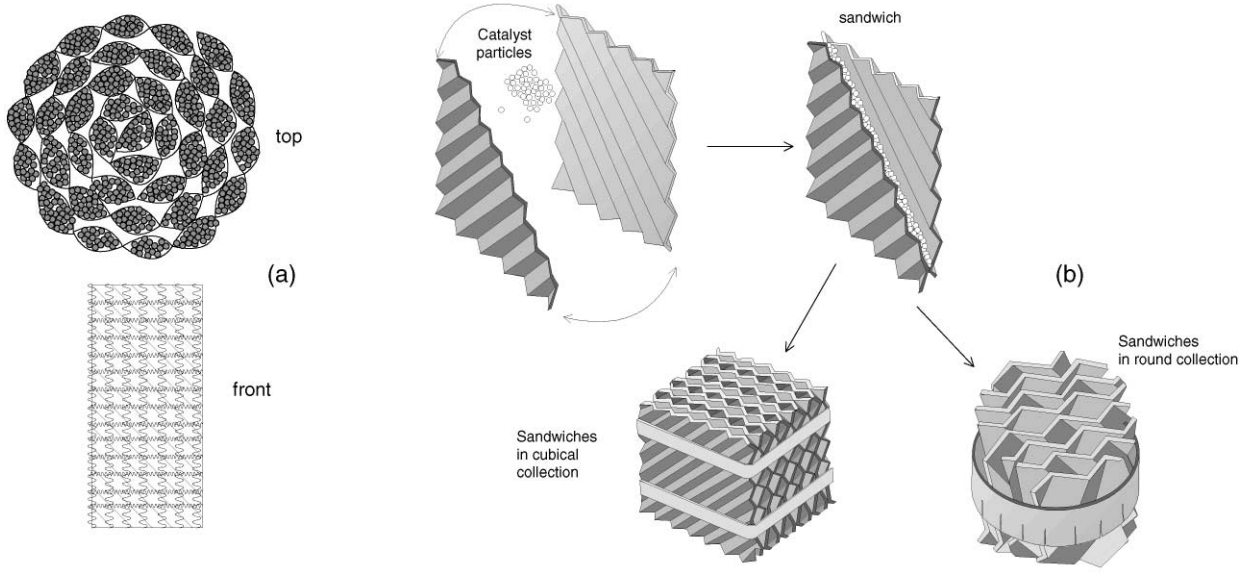

Fig. 1. (a) Catalyst bales licensed by Chemical Research and Licensing. (b) Structured catalyst-sandwiches. Catalyst sandwiched between two corrugated wire gauze sheets, then joined together and sewn on all four sides into a sandwich "configuration", arranged into a cubical collection or round collection.

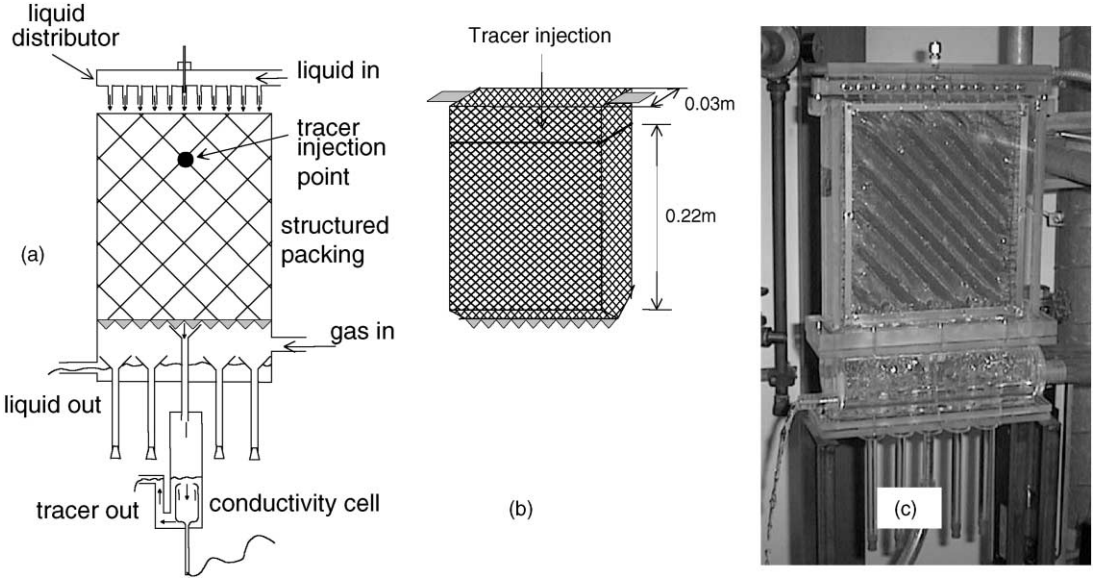

Fig. 2. Experimental set-up for (a) KATAPAK-S structure and (b) conventional packed bed. (c) Photograph of set-up which has a common transparent housing for both (a) and (b).

The relevant details of the KATAPAK-S structure are: Width $W = 0.22$ m; Height $L = 0.290$ m; Depth $B = 0.030$ m; Angle of inclination $= 45^{\circ}$; Volume of 'packed channels' $= 0.775 \times 10^{-3}$ m^3; Specific surface for the gas flow $= 122.3$ m^2/m^3; Diameter of glass beads in 'packed channels', $d_p = 1.0$ mm; Volume of solids (glass beads) $= 0.411 \times 10^{-3}$ m^3.

The relevant details of the packed bed structure are: Width $W = 0.220$ m; Height $L = 0.220$ m; Depth $B = 0.030$ m; Volume of packed bed $= 1.452 \times 10^{-3}$ m^3; Specific surface for the gas flow $= 75.7$ m^2/m^3; Diameter of glass beads, $d_p = 1.0$ mm; Volume of solids (glass beads) $= 0.9 \times 10^{-3}$ m^3.

Fig. 2(c) shows a photograph of the experimental set-up. In order to avoid wall flow a 'sheet' of the packing, either KATAPAK-S or the packed bed, is placed in a rectangular box of polycarbonate (0.29 m × 0.26 m × 0.04 m) in such a way that the sheet does not touch the walls of

the box. At the top of the sheet a liquid distributor is mounted consisting of 11 spray nozzles with an internal diameter of 1.5 mm. A saw-toothed (10 teeth) metal strip, fixed at the bottom of the packed sheet, ensures a uniform outflow of the liquid phase. The liquid at the bottom of the sheet can be sampled with one of the five funnels placed at different lateral positions. The funnels can be moved in the vertical direction. The sampled liquid flows through an electrical conductivity cell and the signal is — after analog-to-digital conversion — stored in a PC with a frequency of 10 Hz. The liquid volume in the conductivity cell is 25 ml.

Further details of the experimental set-up and measurement techniques, including photographs of the rig, are available on our website: http://ct-cr4.chem.uva.nl/strucsim.

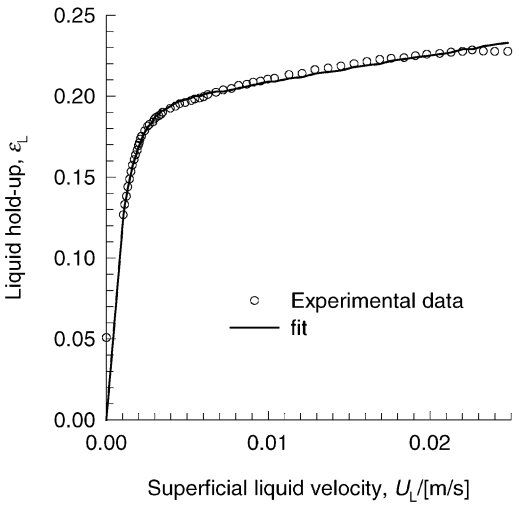

Fig. 3. Experimentally determined liquid hold-up in KATAPAK-S structure.

3. Liquid hold-up measurements

For interpretation of the residence time distribution measurements and determination of the interstitial liquid velocity u_L from the superficial liquid velocity U_L, it is necessary to have information on the liquid hold-up, ε_L. This is defined as the volume V_L of the liquid divided by the volume of the reactor V_R ($= L \times B \times W$). For the measurement of the liquid-phase hold-up ε_L, the set-up as shown in Fig. 1 (without the sampling part at the bottom) is placed on a balance with a range of 0–10 kg with an accuracy of 1 g. The liquid flow rate can be set in a range of $0–0.164 \times 10^{-3}$ m^3/s. The liquid leaving the sheet at the bottom is recycled to a storage tank by means of a drainpipe. The drainpipe is not in contact with the balance. The measurements have been performed without gas flow after it was confirmed that co-current or counter-current gas flow outside the structures had no influence on the liquid hold-up. After subtracting the dry mass from the corrected mass the liquid volume and the liquid hold-up can be calculated. The liquid hold-up data are shown in Fig. 3 for the KATAPAK-S sheet. The superficial liquid velocity is equal to the volumetric liquid flow rate divided by the cross-section A of the packing. For the KATAPAK-S sheet the cross-section is equal to the width times the depth ($B \times W = 0.22$ m $\times$ 0.03 m). A similar set of measurements were also performed for the packed bed.

4. Liquid residence time distribution measurements

The packed sheet was completely wetted at a relatively high-liquid velocity. After that, the desired liquid flow rate was imposed on the system. For two interstitial liquid velocities $u_L = 0.019$ m/s and $u_L = 0.003$ m/s the residence time distributions have been determined in counter-current operation at a high superficial gas velocity $U_G = 1.66$ m/s. No significant effect of the counter-current gas flow on the residence time distribution curves has been observed. Therefore, all the remaining experiments are performed with liquid (water) flow only. Ten seconds after starting the registration of the tracer signal, a small amount (500 μL) of a saturated NaCl solution was injected at the top of the packed sheet. The injection time was less than 0.5 s. The tracer injection point of the packed KATAPAK-S sheet was 40 mm below the top at the horizontal centre. The tracer injection point of the packed bed was at the top at the horizontal centre. This results in a vertical distance H of 0.22 m from the tracer injection point to the bottom of the packing for both systems. Two sets of measurements have been performed: (1) tracer injection into the 'packed channels' of the KATAPAK-S packing (Fig. 2(a)), and (2) tracer injection into the packed bed of the packed bed (Fig. 2(b)).

For each liquid velocity, conductivity was measured at five different lateral positions. Representative RTDs are shown in Figs. 4(a) and (b). Even a first glance at Fig. 4 is sufficient to conclude that the radial dispersion in the criss-crossing structure of the KATAPAK-S packing is significantly higher than in the packed-bed structure. Before proceeding with a quantitative treatment of the RTD experiments we sketch a physical picture of the flow phenomena in the two structures.

4.1. Qualitative description of RTD in KATAPAK-S structure

At low liquid velocities, the liquid is held inside the packed channels by capillary forces and will flow in a more lateral direction, due to the inclination of the packed channels. Above a certain liquid velocity we also observe a liquid film outside the packed structure. As shown in Fig. 5(a), the liquid inside the packed structure

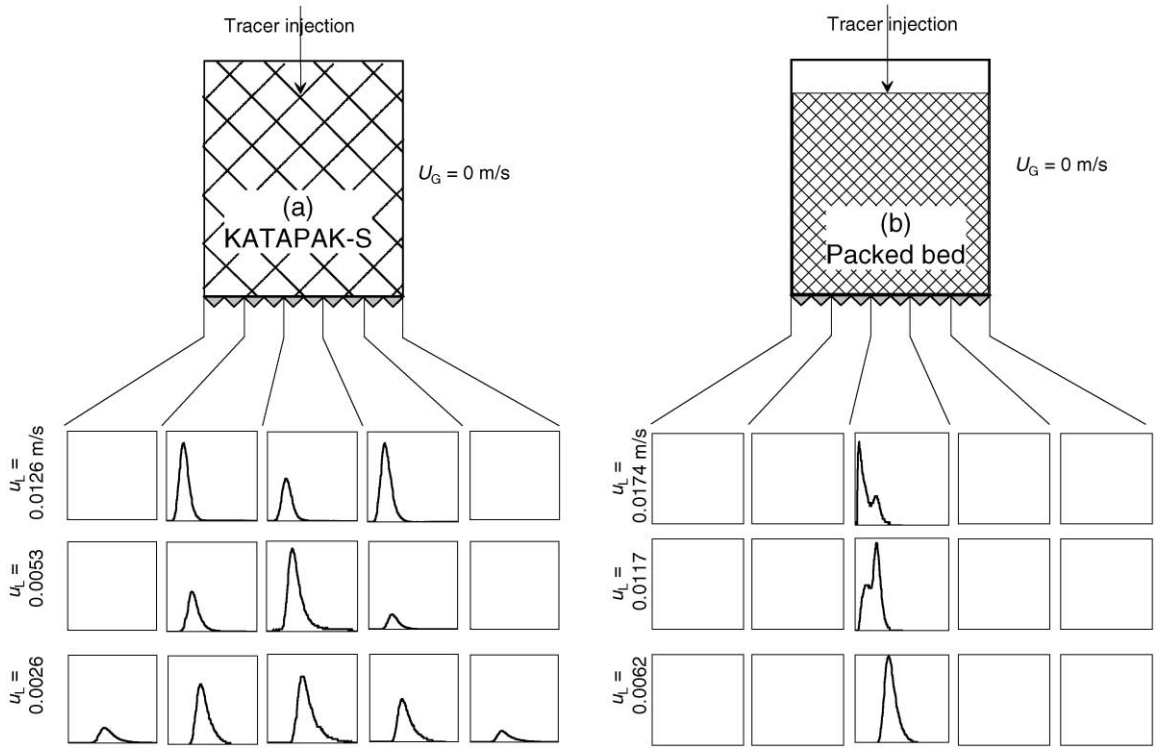

Fig. 4. Typical RTD in (a) KATAPAK-S and (b) packed-bed structures.

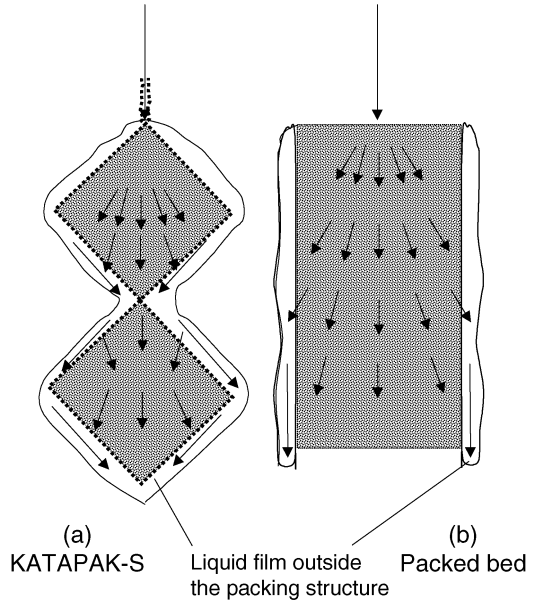

Fig. 5. Qualitative picture of flow in and outside (a) KATAPAK-S and (b) packed-bed structures.

is forced to flow to the wall of the structure. If there is a liquid film outside the packed structure, the tracer will be mixed with this liquid film. The tracer will partly re-enter the next packed channels and partly remain in the relatively fast-flowing liquid film. The specific surface of the KATAPAK-S structure is larger than that of the packed-bed structure. Therefore, the thickness of the liquid film will be smaller. Furthermore, because of the corrugation of the structured packing, this liquid film can re-enter the packing due to its momentum (see Fig. 5(a)). This results in a single peak in the residence time distribution with a relatively long tail compared to the packed-bed structure. A further increase of the liquid flow enhances the velocity of the liquid film outside the packed structure. There is less time for the tracer to re-enter the packed channels. This makes it possible to obtain a higher tracer concentration at off-centre positions than at the centre position.

Due to the bypassing in the fast-flowing liquid film, liquid outside the packed structure will hardly be in contact with the catalyst particles. Therefore, the operation of a structured packed column at high liquid loads is not desired. The approximate liquid velocity at which the liquid starts to bypass the structure is estimated to occur at an interstitial liquid velocity $u_L \approx 0.022$ m/s.

4.2. Qualitative description of RTD in packed bed

At all liquid velocities the tracer flows in an almost vertical direction. At low liquid velocities we obtain a single peak in the RTD, indicative of no by-passing. Above an interstitial liquid velocity $u_L \approx 0.015$ m/s, part

of the liquid flows as a liquid film outside the packed structure. This liquid film has a much higher velocity than the liquid inside the structure, resulting in two peaks in the residence-time distribution. The first peak of this bimodal distribution corresponds to the relatively fast-flowing liquid film outside the packed structure, whereas the second peak corresponds to the residence time distribution of the liquid inside the packing. Unlike the KATAPAK-S structure, the liquid film flowing outside the packed bed cannot re-enter the packing.

5. CFD simulation model development

We attempt now to model the flow of liquid within the criss-crossing structure of KATAPAK-S using computational fluid dynamics (CFD). In the simulations we ignore the gas flowing outside the channels. The first problem in developing a CFD model is to develop the grid structure of a single "sandwich" of KATAPAK-S (Fig. 1(b)). We develop the grid on the basis of a set of intersecting, connecting, triangular tubes ("Toblerone"). As shown in Fig. 6, the computational space is made up of a total of 16 Toblerones with 32 intersections. A single Toblerone is 18 mm high and 36 mm wide. Between two channels there is a 2 mm gap. An irregular grid covers the cross-section of a triangular cross-section. The total grid contains 129,024 cells.

For the purposes of CFD modelling we take the packing inside the criss-crossing structure of Fig. 6 to be isotropic and having a uniform porosity ε. The equations describing the conservation of total mass and momentum are

$$\frac{\partial(\varepsilon\rho_L)}{\partial t} + \nabla\cdot(\rho_L\varepsilon\mathbf{u}_L) = 0 \tag{1}$$

and

$$\frac{\partial(\rho_L\varepsilon\mathbf{u}_L)}{\partial t} + \nabla\cdot(\rho_L\varepsilon\mathbf{u}_L\mathbf{u}_L - \mu_L\varepsilon(\nabla\mathbf{u}_L + (\nabla\mathbf{u}_L)^{\mathrm{T}})) = \varepsilon\mathbf{B} - \varepsilon\nabla p, \tag{2}$$

where $\mathbf{B}$ is the body force describing the resistance to liquid flow offered by the packing. This body force has been modelled using the Ergun equation:

$$\mathbf{B} = \left[150\frac{\mu_L}{d_p^2}\frac{(1-\varepsilon)^2}{\varepsilon^2} + \frac{1.75\rho_L}{d_p}\frac{(1-\varepsilon)}{\varepsilon}|\mathbf{u}_L|\right]\mathbf{u}_L. \tag{3}$$

For describing the diffusion of a tracer the equation of continuity for tracer can be written as

$$\frac{\partial(\varepsilon\rho_L\omega)}{\partial t} + \nabla\cdot(\rho_L\varepsilon\omega\mathbf{u}_L) = \nabla\cdot(\varepsilon\rho_L D\nabla\omega), \tag{4}$$

where ω is the mass fraction of the tracer in the liquid and D is the molecular diffusivity of the tracer. In the simulations we take the properties of water $\rho_L = 998\ \mathrm{kg/m^3}$, $\mu_L = 0.001$ Pa s with tracer diffusivity $D = 1\times 10^{-9}\ \mathrm{m^2/s}$, porosity $\varepsilon = 0.37$ and particle diameter, $d_p = 1$ mm.

At inlets, the values for velocities are explicitly specified. A no-slip condition is used for walls. At the outlets, the pressure is specified. For the velocities, a Neumann boundary condition is being imposed at the outlets:

$$\frac{\partial}{\partial n}u_\perp = 0. \tag{5}$$

The model has been implemented within a commercial CFD package CFX, version 4.2 and simulations have been performed on a Silicon Graphics Power Indigo 2 (R8000 processor) and on a Silicon Graphics O2 (R10000 processor) machine. A typical simulation took about two to three weeks to finish.

Discretisation of the equations at the grid is performed using a finite differencing (finite volume) method. Velocity vector equations are being treated as scalar equations: one scalar equation for each velocity component. All scalar variables are discretised and evaluated at the cell centres. Velocities required at the cell faces are evaluated by applying improved Rhie–Chow interpolation. Transport variables (diffusion coefficients, effective viscosities) are evaluated and stored at the cell faces. The SIMPLEC pressure correction algorithm is being applied.

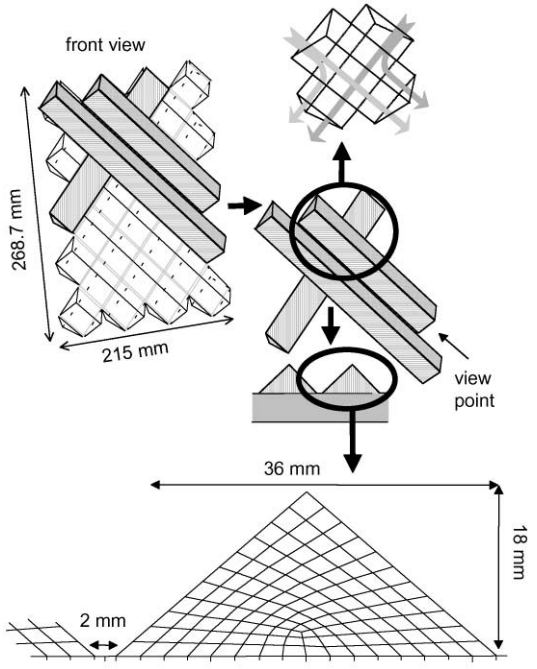

Fig. 6. Computational grid of the KATAPAK-S structure.

The applied time differencing scheme is fully implicit backward. This means the solution at step n is a function of the derivatives at step n and the solution at step $n-1$. Since the derivatives at step n are unknown, this results in a large system of linearised equations to be solved. This system of equations is being solved in an iterative way, using the Stone solver (velocity and volume/mass fraction equations) and the ICCG solver (pressure equation).

The iterative procedure for solving implicit time differencing is referred to as the inner iteration. Per time step 15 inner iterations have been performed. Coupling of the different equations is also addressed in an iterative way. This is referred to as the outer iteration. Time steps of 0.02 s were used in the simulations.

Differencing of the diffusion terms is always handled by central differencing, with a local diffusion coefficient stored at the cell faces. For the advection terms, central differencing is used for pressure. Hybrid differencing is used for all the other equations. In this hybrid scheme central differencing is used for low grid cell Pe numbers ($Pe < 2$) and upwind differencing (ignoring diffusion) is used for high grid cell Pe numbers.

Further computational details, including animations of the tracer simulations, can be viewed on our website: http://ct-cr4.chem.uva.nl/strucsim.

6. CFD simulation results

In the simulations, the liquid enters the system through the top 8 tubes, and flows down through the system to exit at the bottom 8 triangular tubes. Once steady state is obtained, a pulse tracer is injected at the first crossing below the top in the centre of the structure on the top left of Fig. 7. Tracer concentrations at the 8 outlets are constantly monitored to obtain the RTD curves at 8 horizontal positions. For each outlet, the tracer concentration is averaged over the cell volume of the cells that make up the outlet. These obtained curves are used to estimate axial and radial dispersion coefficients. Fig. 7 shows the progression of tracer through the structure with intervals of 1 s for a volumetric liquid flow of 2.2×10^{-5} m^3/s. Typical RTD curves obtained from such a simulation are shown in Fig. 8. For comparison purposes, we also performed one simulation with a packed-bed structure without criss-crossing.

7. Estimation of dispersion coefficients from RTD curves

From the measured and simulated RTD curves shown in Figs. 4 and 8, we estimated both the axial and radial dispersion coefficients using the two-dimensional convective diffusion equation

$$\frac{\partial \omega}{\partial t} = D_{\mathrm{ax}} \frac{\partial^2 \omega}{\partial x^2} - u_L \frac{\partial \omega}{\partial x} + D_{\mathrm{rad}} \frac{\partial^2 \omega}{\partial y^2}, \tag{6}$$

where y is the lateral distance. Eq. (6) can be solved analytically to yield the E-curve

$$E(t) = \frac{LW}{4} \frac{\exp(-(x-u_L t)^2/(4D_{\mathrm{ax}}t))\exp(-y^2/(4D_{\mathrm{rad}}t))}{\pi t \sqrt{D_{\mathrm{ax}} D_{\mathrm{rad}}}}. \tag{7}$$

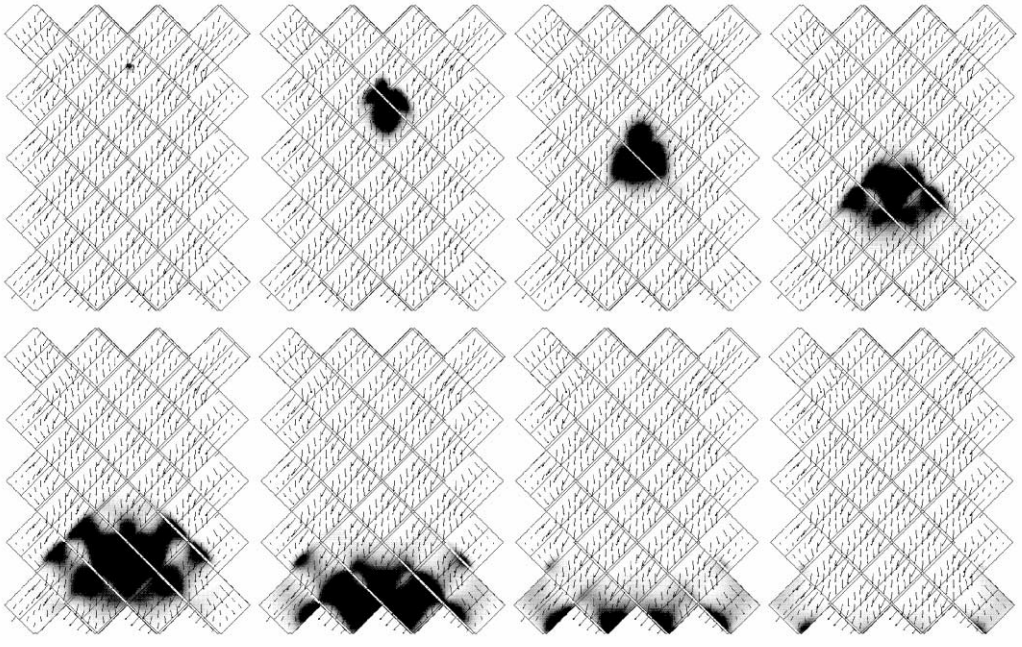

Fig. 7. Snapshots of tracer progression through the computational grid. The arrows denote the velocity vectors of the liquid phase.

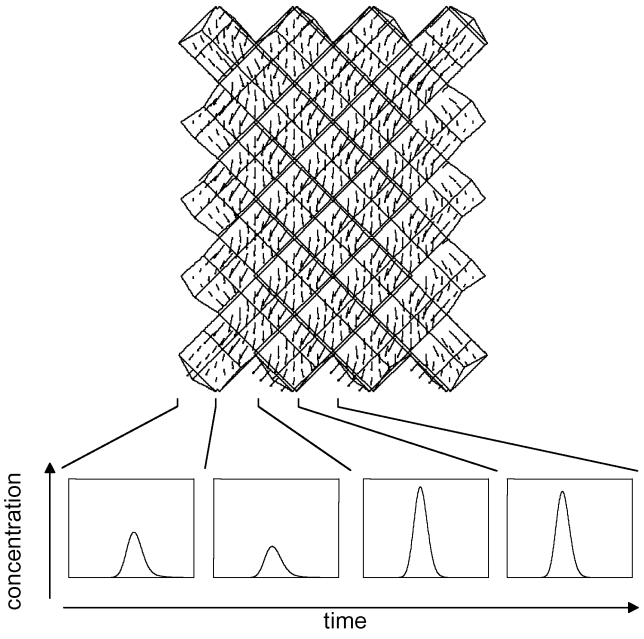

Fig. 8. RTD curves from CFD simulations.

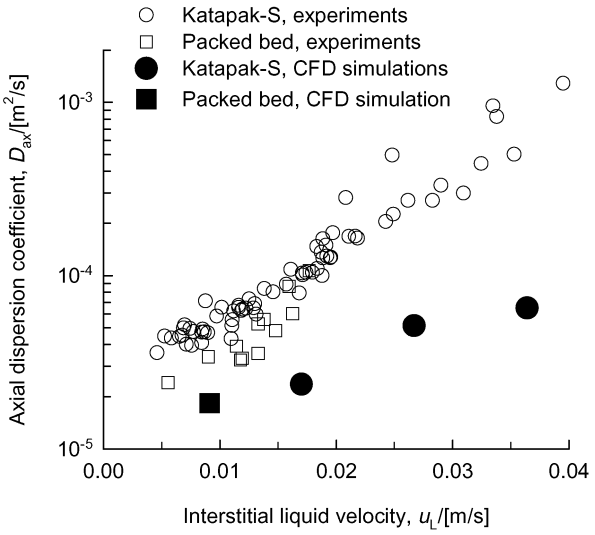

Fig. 9. Axial dispersion coefficients. Experiments vs. simulations.

The two model parameters D_{rad} and D_{ax} are obtained by fitting the simulated curves.

8. Axial and radial dispersion coefficients: experiment vs. CFD simulation

In Fig. 9 the D_{ax}, for experiments and simulations of the KATAPAK-S and packed-bed structures are shown. Both in the experiments and in the simulations the D_{ax} values are comparable for the two structures. We note, however, that the values of D_{ax} from CFD simulations are about an order of magnitude lower than those from experiments. This is because in the experiments we have flow of liquid films on the outside of the structures, leading to enhanced dispersion. In the CFD simulations the walls are modelled as being impermeable. The deviation between the experiments and CFD is a testimony to the existence of liquid flow outside the packing, as shown in Fig. 5. This deviation increases with increasing liquid load.

For the packed bed the dispersion in the lateral direction, both in the experiments (cf. Fig. 4(b)), and in the solitary packed-bed simulation performed, was too small in order to be able to estimate the radial dispersion coefficient D_{rad}. For the KATAPAK-S structure, on the other hand, a significant lateral tracer movement exists (see Figs. 4(a) and 8). The estimated D_{rad} values are shown in Fig. 10. We note that there is good agreement between the CFD simulations and our experiments. The liquid flow outside the packing in the experiment does not distort the value of the (large) lateral dispersion coefficient.

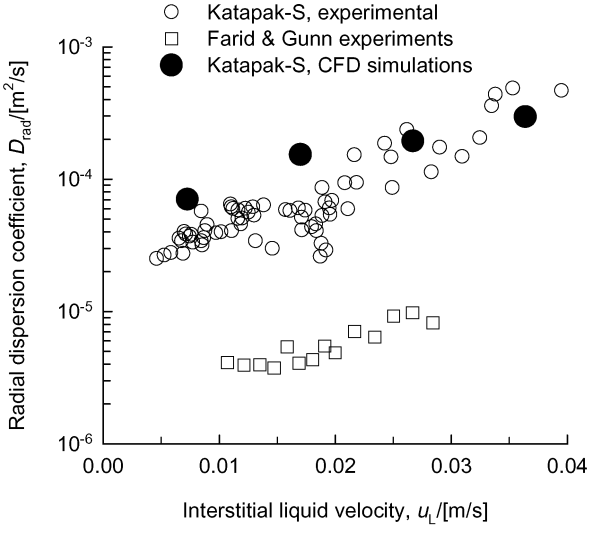

Fig. 10. Radial dispersion coefficients. Experiments vs. simulations. The Farid and Gunn (1979) experiments were carried out in a trickle bed with 2 mm spheres.

Since we were unable to determine D_{rad} for the packed-bed structure (Fig. 4(b)) due to the negligibly small lateral dispersion, we have plotted the published data of Farid and Gunn (1979) for D_{rad} for co-current downflow in trickle beds with particles of 2 mm. The radial dispersion in KATAPAK-S is about an order of magnitude higher than that in trickle beds.

9. Concluding remarks

We set out to compare the dispersion characteristics of KATAPAK-S with a conventional packed bed. The following major conclusions can be drawn from the work presented in this paper.

1. The values of axial dispersion coefficient D_{ax} in these two structures are comparable in magnitude. The mechanism for axial dispersion is governed by mixing processes at the particle scale, which is chosen to be the same in the two cases (1 mm).
2. The values of D_{ax} from CFD simulations are considerably lower than those measured experimentally. The reason for this deviation is the flow of liquid outside the wire-gauze envelopes in practice. This liquid film flow causes considerable dispersion, especially at high liquid loads. Operation at high liquid loads is not desirable from a reactor engineering standpoint.
3. For the KATAPAK-S structure, the radial dispersion coefficient D_{rad} is of the same order of magnitude as the axial dispersion coefficient D_{ax} (cf. Figs. 9 and 10).
4. The values of D_{rad} obtained from experiment and CFD simulations are comparable. Evidently, the phenomenon of liquid flow outside the packing does not significantly distort the radial dispersion characteristics.
5. The value of D_{rad} for KATAPAK-S is about one order of magnitude higher than that in co-current down flow trickle beds. This is considered to be a desirable feature of the criss-crossing structures because excellent radial dispersion will prevent the formation of hot spots in the reactor.

Notation

A	area, m
B	depth, m
$\mathbf{B}$	body force, N/m^3
d	diameter, m
D	diffusivity of tracer in the liquid, m^2/s
D_{ax}	axial dispersion coefficient, m^2/s
D_{rad}	radial dispersion coefficient, m^2/s
E	E-curve
g	gravitational constant, m^2/s
L	length, m
p	pressure, Pa
Pe	Péclet number
R	flow resistance, kg/m^3/s
t	time, s
u	interstitial velocity, m/s
U	superficial velocity, m/s
V	volume, m^3
W	width, m
x	axial position, m
y	radial position, m
z	depth, m

Greek letters

ε	volume porosity/hold-up
μ	viscosity, Pa s
ρ	density, kg/m^3
ω	mass fraction of tracer, dimensionless

Subscripts

ax	axial
G	gas phase
L	liquid phase
p	particle
R	reactor
rad	radial

Acknowledgements

Financial assistance from The Netherlands Organization for Scientific Research (NWO) in the form of a "programmasubsidie" to RK is gratefully acknowledged. JMvB is also grateful to NWO for grant of a PhD fellowship. The KATAPAK-S® structure used in this research was made available by Sulzer Chemtech Ltd., Switzerland.

References

Bart, H. -J., & Landschützer, H. (1996). Heterogene Reaktivdestillation mit axialer Rückvermischung. *Chemie Ingenieur Technik*, *68*, 944–946.

DeGarmo, J. L., Parulekar, V. N., & Pinjala, V. (1992). Consider reactive distillation. *Chemical Engineering Progress*, *3*, 43–50.

Ellenberger, J., & Krishna, R. (1999). Counter-current operation of structured catalytically packed distillation columns: pressure drop, hold-up and mixing. *Chemical Engineering Science*, *54*, 1339–1345.

Farid, M. M., & Gunn, D. J. (1979). Dispersion in trickle and two-phase flow in packed columns. *Chemical Engineering Science*, *34*, 579–592.

Gelbein, A. P., & Buchholz, M. (1991). *Process and structure for effecting catalytic reactions in distillation structure*. U.S. Patent 5073236.

Higler, A. P., Krishna, R., Ellenberger, J., & Taylor, R. (1999). Counter-current operation of a structured catalytically packed bed reactor: Liquid-phase mixing and mass transfer. *Chemical Engineering Science*, *54*, 5145–5152.

Johnson, K. H., & Dallas, A. B. (1994). *Catalytic distillation structure*. U.S. Patent 5348710.

Moritz, P., & Hasse, H. (1999). Fluid dynamics in reactive distillation packing KATAPAK®-S. *Chemical Engineering Science*, *54*, 1367–1374.

Smith Jr., L. A. (1985). *Catalytic distillation process and catalyst*. European Patent 008860B1.

Stringaro, J. P. (1991). *Reactor including a catalyst body for performing a heterogeneous reaction*. European Patent 433222A1.

Stringaro, J. P. (1995). *Catalyzing fixed bed reactor*. U.S. Patent 5470542.

Subawalla, H., Gonzalez, J. C., Seibert, A. F., & Fair, J. R. (1997). Capacity and efficiency of reactive distillation bale packing: modeling and experimental validation. *Industrial and Engineering Chemistry Research*, *36*, 3821–3832.

Taylor, R., & Krishna, R., (2000). Modelling reactive distillation, *Chemical Engineering Science*, *55*, 5183–5229.

Van Gulijk, C. (1998). Using computational fluid dynamics to calculate transversal dispersion in a structured packed bed. *Computers and Chemical Engineering*, *22*, S767–S770.